



OPEN ACCESS

International Journal of Bifurcation and Chaos, Vol. 31, No. 4 (2021) 2150110 (12 pages)

© The Author(s)

DOI: 10.1142/S0218127421501108

Locating and Stabilizing Unstable Periodic Orbits Embedded in the Horseshoe Map

Yuu Miino

*Tokyo University of Technology, 1404-1, Uchikoshimachi,
Hachioji, Tokyo, Japan
miinoy@stf.teu.ac.jp*

Daisuke Ito

*Gifu University, 1-1, Yanagido, Gifu, Japan
d_ito@gifu-u.ac.jp*

Tetsushi Ueta

*Tokushima University,
2-1, Minamijosanjima-cho, Tokushima, Japan
ueta@tokushima-u.ac.jp*

Hiroshi Kawakami

Tokushima University, Japan

Received January 6, 2021

Based on the theory of symbolic dynamical systems, we propose a novel computation method to locate and stabilize the unstable periodic points (UPPs) in a two-dimensional dynamical system with a Smale horseshoe. This method directly implies a new framework for controlling chaos. By introducing the subset based correspondence between a planar dynamical system and a symbolic dynamical system, we locate regions sectioned by stable and unstable manifolds comprehensively and identify the specified region containing a UPP with the particular period. Then Newton's method compensates the accurate location of the UPP with the regional information as an initial estimation. On the other hand, the external force control (EFC) is known as an effective method to stabilize the UPPs. By applying the EFC to the located UPPs, robust controlling chaos is realized. In this framework, we never use *ad hoc* approaches to find target UPPs in the given chaotic set. Moreover, the method can stabilize UPPs with the specified period regardless of the situation where the targeted chaotic set is attractive. As illustrative numerical experiments, we locate and stabilize UPPs and the corresponding unstable periodic orbits in a horseshoe structure of the Duffing equation. In spite of the strong instability of UPPs, the controlled orbit is robust and the control input retains being tiny in magnitude.

Keywords: Chaos; horseshoe map; symbolic dynamics; unstable periodic point; numerical computation; controlling chaos.

This is an Open Access article published by World Scientific Publishing Company. It is distributed under the terms of the Creative Commons Attribution 4.0 (CC BY) License which permits use, distribution and reproduction in any medium, provided the original work is properly cited.

1. Introduction

After the discovery of chaos, researchers have discussed considerably the applications to practical situations: encryption of the data in communication technology or in signal processing [Habutsu *et al.*, 1990; Stojanovski & Kocarev, 2001], neural networks [Aihara *et al.*, 1990], water quality forecast in environmental engineering [Huang *et al.*, 2008], electromagnetic interference suppression in electronics, and so on. On the other hand, some researchers have also considered how to suppress the chaos, called the controlling chaos, because chaos is undesirable in many cases due to its randomness, noisiness, and unpredictability. The typical and also famous examples of the method to control chaos are OGY method [Ott *et al.*, 1990], external force control (EFC) [Pyragas, 1992], and delayed feedback control (DFC) [Kittel *et al.*, 1995; Nakajima, 1997]. Even though there have been many other controlling methods developed [Rajasekar & Lakshmanan, 1993; Myneni *et al.*, 1999; Zambrano & Sanjuán, 2009; Sabuco *et al.*, 2010], much studies have still relied on these legacy methods [Yi *et al.*, 2019; Ueta *et al.*, 2015; Mahmoud *et al.*, 2017]. However, for using these three methods, we have to take care of some points. OGY method requires the unstable periodic point (UPP) corresponding to an unstable periodic orbit (UPO) embedded within the chaotic attractor in advance. While for EFC, we should select a target orbit, which is often the analytical solution of nonlinear differential equation and thus hard to explicitly calculate. On DFC, we cannot predict which orbit the chaos converges to. Discussing controlling chaos to an arbitrary orbit, the analysis of orbits in chaos is one of the most effective ways. Indeed, some studies, such as [Faranos, 1995], have proposed computational methods to calculate the exact trajectory for certain UPOs. Nevertheless, it is still not easy to locate an arbitrary UPP globally embedded in the state space because almost all of these studies focus on the local property of the UPP.

On the other hand, the studies on symbolic dynamical systems have unveiled a lot of facts about chaos. Among them, Smale [2000] has proved one criterion causing chaos: chaos arises for transversal homoclinicity of manifolds of periodic point, when introducing a Smale horseshoe, which is topologically conjugate to a symbolic dynamical system called a full 2-shift. His research has also shown that horseshoe includes a countably infinite set

containing 2^ℓ periodic points with period- ℓ and an uncountably infinite set containing nonperiodic points. These properties are now well known as the common property of chaotic systems. A symbolic dynamical system is one of the simplest dynamical systems having less information than the general systems, that is, it does not possess the dimension, the stability of the state, and so on. However, it brings many remarkable facts common to the conjugate systems. Thus, we are certain that the symbolic dynamical system is a key to develop general locating methods of UPPs.

Symbolic dynamical systems contain a topological relationship among the periodic states in its domain. In other words, a symbolic dynamical system has the information of the positions of an arbitrary UPP globally embedded in the state space. This structure is invariant under homeomorphism, so a conjugate system to the original symbolic system also contains the same topology. Even better, this structure is independent of whether the chaotic state is attractive or not, which implies that we can find UPPs also in the transient chaos. We have considered that these facts help to locate all UPPs in the chaotic behavior of planar dynamical systems. Furthermore, the corresponding UPO should be suitable to the controlling methods such that OGY or EFC. From the previous research [Ueta *et al.*, 2015], we know EFC works well in determining the target orbit. Besides, comparing with OGY, EFC can perform with better robustness. Thus, in this paper, from the standpoint of symbolic dynamics, we try to investigate a computation method to locate arbitrary UPPs and stabilize them by using EFC method.

This paper composes of five parts. In Sec. 1, we confirmed the motivation of our study. In Sec. 2, let us define some preliminaries for our novel method. We take a general definition for a two-dimensional nonlinear map constructing a discrete-time dynamical system and confirm the topological types of the periodic points in the state space of the system. Besides, we introduce a Smale horseshoe geometrically with its primal domain S . Basic ideas for symbolic dynamical systems, e.g. shift map, symbolic sequence, full 2-shift, and so on, are also included in this section. Also, we verify the homeomorphism between a horseshoe map and a full 2-shift. In Sec. 3, we suggest a method that locates a particular UPP of a horseshoe map intentionally. We carefully describe the principle of why our method

is valid for the map according to the dynamical property of symbolic systems. With some new definitions for subsets of a horseshoe in a symbolic system and corresponding discrete-time map, we locate the region where the UPP belongs. We also try to mention the robustness of the method by using the distance d defined in the space of symbolic sequences. In the last part of Sec. 4, we give a step-by-step procedure for our novel method. In the earlier part of Sec. 4, we present the results of numerical experiments for a continuous-time planar system: Duffing equation [Kovacic & Brennan, 2011]. As a result, we find our method guarantees that we can locate the initial condition candidate of Newton’s method to find a periodic point. Moreover, we confirm whether the method derives the periodic points correctly within the given errors. In the latter part, we show a result of EFC control using the UPO corresponding to the obtained UPP. We conduct the numerical experiments for the Duffing equation again and find whether the UPOs are proper target orbits or not from the standpoint of the convergence of the control input. In Sec. 5, we conclude this study.

2. System Description

2.1. Two-dimensional map with Smale horseshoe

Let us consider a nonlinear two-dimensional diffeomorphism T :

$$T : \mathbb{R}^2 \rightarrow \mathbb{R}^2; \quad \mathbf{x} \mapsto T(\mathbf{x}), \quad (1)$$

where $\mathbf{x} \in \mathbb{R}^2$. A kind of map T often describes a discrete-time dynamical system: $\mathbf{x}_{i+1} = T(\mathbf{x}_i)$, $i \in \mathbb{Z}$; then the sequence $(\mathbf{x}_i)_{i \in \mathbb{Z}}$ for \mathbf{x}_0 is a *trajectory* of the system along with \mathbf{x}_0 . A point \mathbf{p} is a fixed point of T if

$$T(\mathbf{p}) = \mathbf{p}. \quad (2)$$

Also, \mathbf{p} is a periodic point with period- ℓ if it satisfies $T^\ell(\mathbf{p}) = \mathbf{p}$ for $\ell \in \mathbb{N}$. For simplicity, we call these points ℓ -periodic points. Jacobian matrix $DT(\mathbf{x})$, which is the derivative of T with respect to \mathbf{x} , represents the asymptotic stability of a fixed point. A fixed point \mathbf{p} is

- a completely stable node if $\|\mu_1\| < 1$ and $\|\mu_2\| < 1$;
- a directly unstable saddle if $-1 < \mu_1 < 1 < \mu_2$;
- a directly unstable saddle if $\mu_1 < -1 < \mu_2 < 1$; and

- a completely unstable node if $\|\mu_1\| > 1$ and $\|\mu_2\| > 1$,

where μ_1 and μ_2 are the eigenvalues of $DT(\mathbf{p})$ ($\mu_1 < \mu_2$). In this paper, we do not take into account the nonhyperbolic points, i.e. there exists i such that $\|\mu_i\| = 1$.

The discrete-time system for T behaves chaotically if T constructs a Smale horseshoe. Smale horseshoe is the topological structure composed of a map T and a subset S of its domain. Suppose that T and S form a Smale horseshoe and S composes of five individual subsets: A , B , C , D , and E with $S \cap T[B] \neq \emptyset$, $S \cap T[D] \neq \emptyset$, and $T[A] \cap S = T[C] \cap S = T[E] \cap S = \emptyset$, where $T[X] = \{T(x) \mid x \in X\}$, Fig. 1 gives a brief example of a Smale horseshoe. Through squishing, stretching, and folding, the area S transforms into the shape like a horseshoe. The inverse map T^{-1} of T also makes the horseshoe structure from the same S but $T^{-1}[S]$ results in another horseshoe, which is topologically symmetric to $T[S]$. We call a set $\Lambda \subset \mathbb{R}^2$ a *horseshoe*, which is the set of points remaining in $B \cup D$ after the infinite-time iteration of T and T^{-1} :

$$\Lambda = \{\mathbf{x} \mid T^n(\mathbf{x}) \in B \cup D \text{ for all } n \in \mathbb{Z}\}, \quad (3)$$

and T is a *horseshoe map*. Horseshoe is homeomorphic to the Cantor set and embeds a countably infinite set of unstable ℓ -periodic points and an uncountably infinite set of nonperiodic trajectories.

2.2. Symbolic dynamical system

A symbolic dynamical system composes of a shift map σ and a bi-infinite sequences space as an evolution equation and a state space, respectively. Assume that two symbols “0” and “1” formulate the space Σ of the bi-infinite sequences:

$$\Sigma = \{(a_i)_{i \in \mathbb{Z}} \mid a_i \in \{0, 1\} \text{ for all } i \in \mathbb{Z}\}, \quad (4)$$

and the shift σ moves each symbol in $a = (a_i)$ as

$$\sigma : \Sigma \rightarrow \Sigma; \quad a = (a_i) \mapsto \sigma(a) = (a_{i+1}). \quad (5)$$

This symbolic system is called a *full 2-shift*. In this paper, we might represent the sequences $(a_i)_{i \in \mathbb{Z}}$ without commas as $(\cdots a_{-2} a_{-1} a_0 a_1 a_2 \cdots)$ and so on. Generally, we locate a decimal point “.” to distinguish a sequence into two parts: a_i for $i \leq 0$ and a_i for $0 < i$. For instance, if $a = (\cdots 000.111 \cdots)$, $\sigma(a) = (\cdots 0001.11 \cdots)$ so that the map σ shifts the

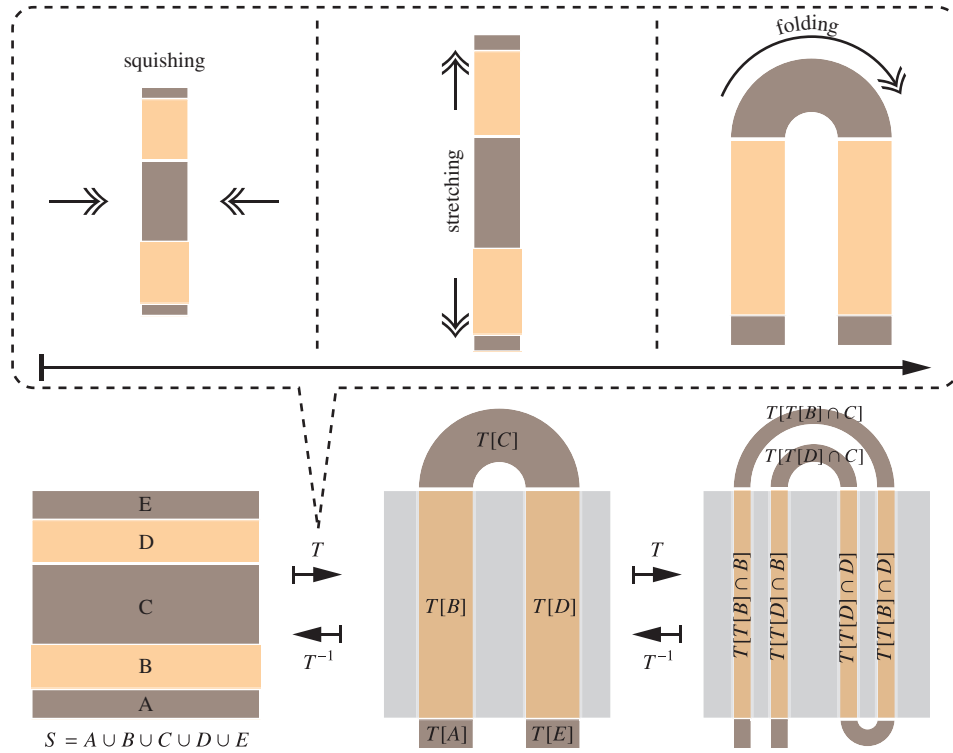


Fig. 1. Schematic illustration for a Smale horseshoe.

decimal point one slot rightward. A sequence $s \in \Sigma$ is a fixed sequence of σ if

$$\sigma(s) = s. \tag{6}$$

Besides, s is a periodic sequence with period- ℓ if it satisfies $\sigma^\ell(s) = s$. The periodic sequences infinitely repeat the same finite symbolic sequence like “01,” “001,” and so on. We name such a sequence a *basic sequence*. Table 1 shows some examples of the periodic sequences and corresponding basic sequences. Notice that some different periodic sequences, like $(\dots 101.010\dots)$ and $(\dots 010.101\dots)$, could have the same basic sequence. From the standpoint of the dynamical system, we can regard these sequences are identical without loss of generality.

Table 1. Examples of ℓ -periodic sequences of σ and their corresponding basic sequence.

| ℓ | Periodic Sequence | Basic Sequence |
|--------|--------------------------|----------------|
| 1 | $(\dots 0000.0000\dots)$ | (0) |
| 1 | $(\dots 1111.1111\dots)$ | (1) |
| 2 | $(\dots 0101.0101\dots)$ | (01) |
| 3 | $(\dots 1001.0010\dots)$ | (001) |
| 3 | $(\dots 1011.0110\dots)$ | (011) |

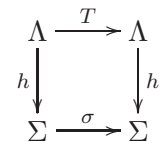
Considering a homeomorphism h :

$$h : \Lambda \rightarrow \Sigma; \quad \mathbf{x} \mapsto (a_i)_{i \in \mathbb{Z}}, \tag{7}$$

where

$$a_i = \begin{cases} 0 & \text{if } T^i(\mathbf{x}) \in B, \\ 1 & \text{if } T^i(\mathbf{x}) \in D, \end{cases} \tag{8}$$

for all $i \in \mathbb{Z}$, then a horseshoe map T and a full 2-shift σ are topologically conjugate to each other with the following diagram:



In other words, every dynamical property of σ is equivalent to the property of T , and vice versa.

As remarkable facts of the full 2-shift, it includes 2^ℓ -periodic sequences with period- ℓ if we distinguish the cases with the same basic sequences. These sequences correspond to the countably-infinite set of periodic points of the horseshoe map. On the other hand, suppose that the distance d

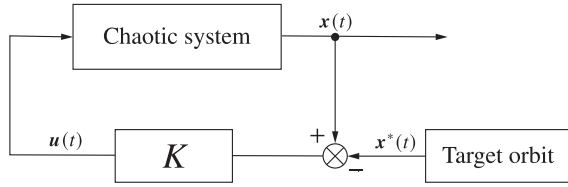


Fig. 2. EFC block diagram.

between two sequences s and s' is

$$d(s, s') = \sum_{i \in \mathbb{Z}} \frac{\delta_i}{2^{|i|}}, \quad (9)$$

where $\delta_i = 0$ if $s_i = s'_i$ and otherwise $\delta_i = 1$, we can find an arbitrarily “near” sequence s' to s satisfying $d(s, s') < \epsilon$ for all $\epsilon > 0$. The set of these dense trajectories correspond to the uncountably-infinite set of nonperiodic trajectories of the horseshoe map.

2.3. External force control

External force control (EFC) is a method to control from the chaotic state to the steady state like with the periodic orbit [Pyragas, 1992]. This method requires a target orbit to construct the control input as shown in Fig. 2. According to our method in Sec. 3, we provide the unstable periodic orbit (UPO), which corresponds to the UPP, as the target orbit of EFC. Adding the controlling part of the EFC, the original chaotic system becomes such that $d\mathbf{x}/dt = \mathbf{f}(t, \mathbf{x})$ changes its form as follows

$$\frac{d\mathbf{x}}{dt} = \mathbf{f}(t, \mathbf{x}) + \mathbf{u}(t), \quad (10)$$

where

$$\mathbf{u}(t) = K(\mathbf{x}(t) - \mathbf{x}^*(t)) \quad (11)$$

is the control input calculated from the current state value and the target orbit.

3. Method to Obtain UPP

Our method to obtain unstable periodic points (UPPs) of T is based on symbolic dynamics. Generally, as mentioned in the previous section, we accept the correspondence between a UPP of T and a periodic-sequence s of σ . Instead, we introduce the definition for a subset-based-correspondence.

Considering a full 2-shift, let us pick up a “bi-finite” ℓ -periodic-sequence b from a “bi-infinite” ℓ -periodic sequence, i.e. there exists $k \in \mathbb{N}$ such that

$$b = (b_i)_{i \in [-k\ell, k\ell-1]}. \quad (12)$$

From the definition, it is clear that b comprises $2k$ basic sequences with period- ℓ . Then, some sequences in Σ completely include b and such sequences assemble one subset $\mathcal{S} \subset \Sigma$:

$$\mathcal{S}(b) = \{(a_i)_{i \in \mathbb{Z}} \mid a_i = b_i \text{ for all } i \in [-k\ell, k\ell - 1]\}. \quad (13)$$

Table 2 shows the example of sequences in $\mathcal{S}(b)$ with $b = (01.01)$, which is a bi-finite two-periodic sequence with $k = 1$. As a matter of course, $\mathcal{S}(b)$ includes an ℓ -periodic sequence corresponding to b and also includes uncountably many trajectories “near” the periodic sequence.

From Eqs. (7) and (8), the preimage of $s \in \mathcal{S}(b)$ under h constructs a subset $\mathcal{R}(b) \subset \Lambda$:

$$\mathcal{R}(b) = h^{-1}[\mathcal{S}(b)] = \{h^{-1}(s) \mid s \in \mathcal{S}(b)\}. \quad (14)$$

In \mathbb{R}^2 , $\mathcal{R}(b)$ gives an infinitely dense but not simply connected region. Although we have no idea to specify $\mathcal{R}(b)$ analytically, we can compute a similar simply connected region $R(b)$ that completely contains $\mathcal{R}(b)$. Since b on $\mathcal{S}(b)$ justifies Eq. (12), \mathbf{x} in $\mathcal{R}(b)$ also satisfies the equivalent limitation: for all trajectories $(\mathbf{x}_i)_{i \in \mathbb{Z}}$ in $\mathcal{R}(b)$, $\mathbf{x}_i \in B$ for i with $b_i = 0$ and $\mathbf{x}_i \in D$ for i with $b_i = 1$. Revisiting the example of $b = (01.01)$, this rule indicates that all trajectories in $\mathcal{R}(b)$ must satisfy $\mathbf{x}_{-2} \in B$, $\mathbf{x}_{-1} \in D$, $\mathbf{x}_0 \in B$, and $\mathbf{x}_1 \in D$. In other words, all \mathbf{x}_0 , including a two-periodic point corresponding to the basic sequence (01), should be in the set $\{T^2[B] \cap T[D] \cap [B] \cap T^{-1}[D]\}$. Consequently, defining $R(b)$ by

$$R(b) = \bigcap_{i=-k\ell}^{k\ell-1} T^{-i}[X_i], \quad (15)$$

where

$$X_i = \begin{cases} B & \text{if } b_i = 0, \\ D & \text{if } b_i = 1, \end{cases} \quad (16)$$

we obtain the relationship $\mathcal{R}(b) \subset R(b)$. The bottom figure of Fig. 3 shows the example of $R(b)$ with

 Table 2. Some sequences of $\mathcal{S}(b)$ with $b = (01.01)$.

| a_i with $i < -2$ | $a_{-2}a_{-1}.a_0a_1$ | a_i with $1 < i$ |
|---------------------|-----------------------|--------------------|
| ...0100 | 01.01 | 1000... |
| ...0001 | 01.01 | 0100... |
| ...0011 | 01.01 | 0100... |
| ...0111 | 01.01 | 1000... |
| ... | 01.01 | ... |

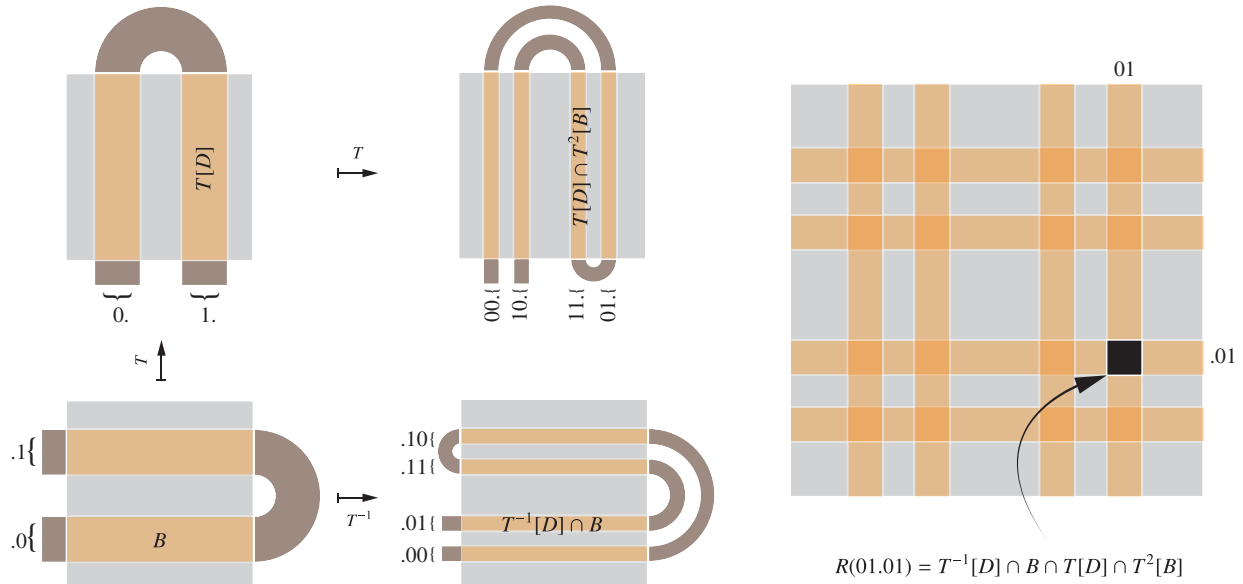


Fig. 3. Schematic illustration of $R(b)$ with $b = (01.01)$.

$b = (01.01)$, which is the common set of primal four sets shown in the top figure.

In the topological sense, we can locate $R(b)$ easily by assigning the symbols to the vertical and horizontal stripes in the area S , as shown by the orange regions in the top four figures in Fig. 3. For vertical stripes, let the first stripes be $T[B]$ and $T[D]$ with the symbols of “0.” and “1.”, respectively, second stripes be the intersection of the first stripes and its image under T , the remaining stripes are also similar. Adding a symbol “0” or “1” to the existing symbolic sequence from the left side, we can make a new symbolic sequence of the second or the following stripes. We determine such a symbol (“0” or “1”) according to where its preimage is located, i.e. $T[B]$ or $T[D]$, respectively. Almost the same discussion is available for T^{-1} , by paying attention to that we should choose the first stripes as B and D and should add the symbol from the right side of the decimal point.

$R(b)$ contains not only the ℓ -periodic point corresponding to the basic sequence b but also the initial point of the uncountably many trajectories “near” the periodic point. This leads us to consider the legacy numerical computation for finding the periodic point, e.g. Newton’s method, which will work fine by giving initial conditions in $R(b)$. On the other hand, improving the value of k , we can take an arbitrarily small value of the distance among the sequences in $\mathcal{S}(b)$ such that $d \leq 1/2^{k\ell}$. Therefore, we can locate a more limited region including periodic

points with the larger k , e.g. $b = (0101.0101)$ and so on.

In summary, our method takes the following steps:

- (1) Find the area $S \subset \mathbb{R}^2$ forming a Smale horseshoe;
- (2) Decide the sequence b of the target UPP with the value of k ;
- (3) Locate $R(b)$ in \mathbb{R}^2 ; and
- (4) Calculate the target UPP by solving Eq. (2) with the initial point in $R(b)$.

For the fourth step, we use Newton’s method until the 2-norm of the left-hand side of Eq. (2) converges within 10^{-10} or the iteration goes over 10.

4. Result of Numerical Experiments

4.1. Obtaining UPO

In this section, let us do a numerical experiment for the Duffing equation, and evaluate our novel method.

Duffing equation models a certain damped and driven oscillator written as

$$\frac{d^2x}{dt^2} + \kappa \frac{dx}{dt} + x^3 = \gamma_0 + \gamma \cos t,$$

where x is the state variable, t is the time, and the others κ, γ_0 , and γ are parameters. Substituting $y = dx/dt$, we rewrite the Duffing equation

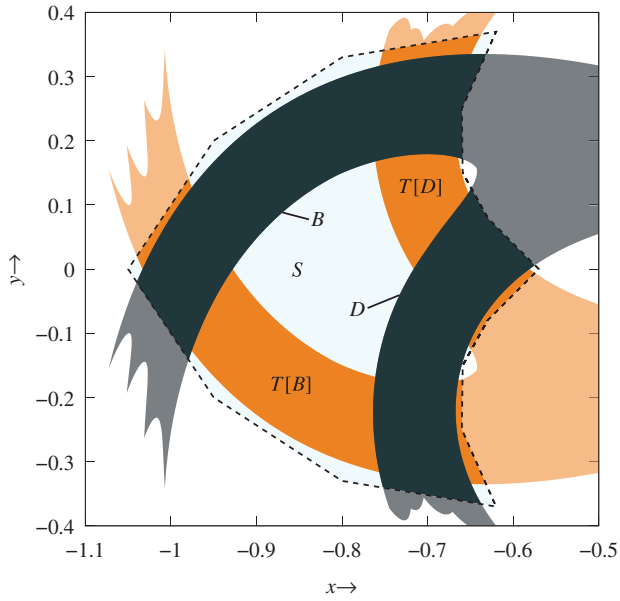


Fig. 4. S , B , D , $T[B]$, and $T[D]$ for Poincaré map T of Duffing equation.

as a two-dimensional nonautonomous dynamical system:

$$\frac{dx}{dt} = y, \quad \frac{dy}{dt} = -\kappa y - x^3 + \gamma_0 + \gamma \cos t. \quad (17)$$

We accept the vector notation like $\mathbf{x} = (x, y)$, and so on. Suppose that Eq. (17) has a solution

$\mathbf{x}(t) = \varphi(t, \mathbf{x}_0)$ with $\mathbf{x}(0) = \varphi(0, \mathbf{x}_0) = \mathbf{x}_0$. For the nonautonomous system including a periodic function of t , we can define stroboscopic mapping as the corresponding Poincaré map:

$$T : \mathbb{R}^2 \rightarrow \mathbb{R}^2; \quad \mathbf{x} \mapsto T(\mathbf{x}) = \varphi(2\pi, \mathbf{x}). \quad (18)$$

Consequently, the discrete-time dynamical system $\mathbf{x}_{n+1} = T(\mathbf{x}_n)$ with this Poincaré map T has the same dynamical property as Duffing equation and we consider this T with the following parameters: $\kappa = 0$, $\gamma_0 = 0.08$, and $\gamma = 0.3$. Thereby, T obtains a symmetry under the transformation of $(t, x, y) \rightarrow (-t, x, -y)$ so that any geometrical feature observed in the state space looks symmetric to $y = 0$. Considering a simply connected region S having the following 16 vertices:

- $(-1.05, 0), (-0.95, \pm 0.2), (-0.83, \pm 0.31),$
- $(-0.75, \pm 0.34), (-0.64, \pm 0.356), (-0.665, \pm 0.25),$
- $(-0.66, \pm 0.15), (-0.63, \pm 0.08), (-0.57, 0),$

T and S form a Smale horseshoe. This S is estimated from the stable and unstable manifolds of the saddle $\mathbf{x}_0 = (-1.029952, 0)$. S does not shape up as a square but it is not due to applying the method. This S and corresponding B , D , $T[B]$, and $T[D]$ are shown in Fig. 4.

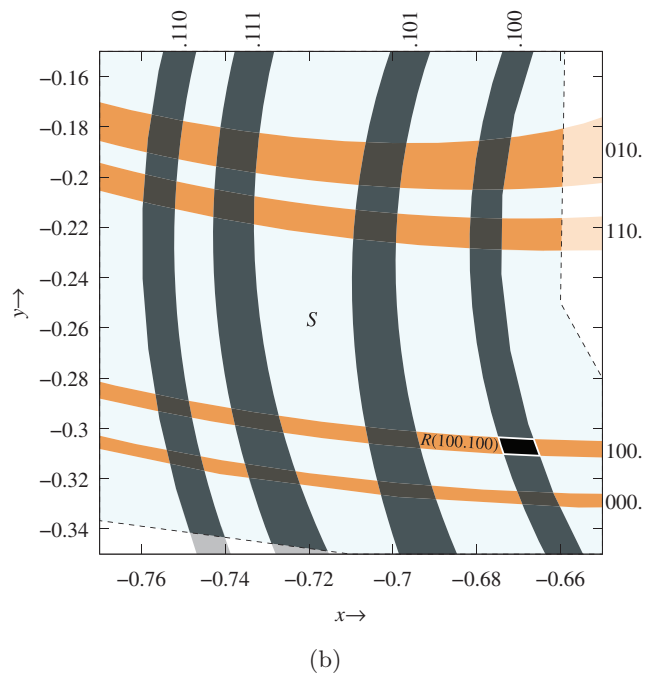
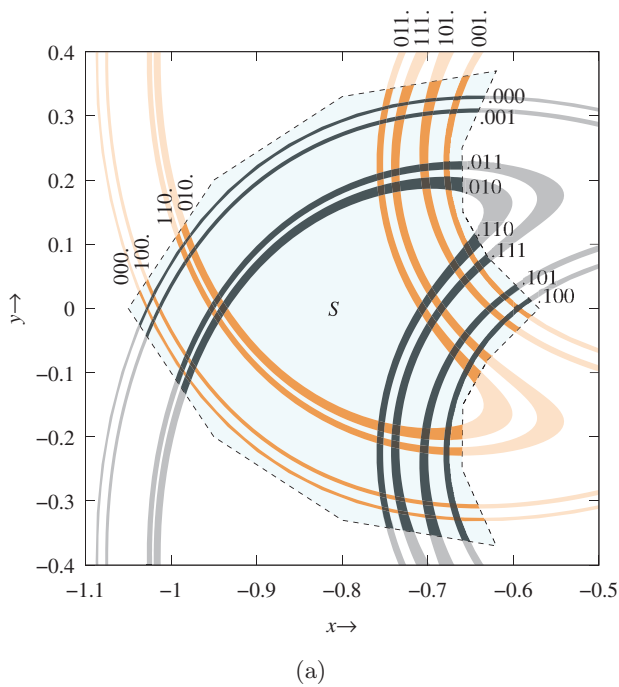


Fig. 5. (a) S (in cyan) and its images under T^3 (in orange) and T^{-3} (in teal) for the Poincaré map of Duffing equation, and (b) its enlargement.

Table 3. Results of experiments on the Poincaré map of Duffing equation — Selected initial condition \mathbf{x}_0 , iteration count of Newton’s method, and error in 2-norm $\|\mathbf{x}_0 - \mathbf{p}\|$ for each b .

| b | \mathbf{x}_0 | Count | $\ \mathbf{x}_0 - \mathbf{p}\ $ |
|-----------|------------------|-------|---------------------------------|
| (000.000) | (−1.020, +0.000) | 4 | 9.951934×10^{-3} |
| (001.001) | (−0.670, +0.307) | 6 | 4.638147×10^{-3} |
| (010.010) | (−0.935, +0.000) | 4 | 9.390133×10^{-4} |
| (011.011) | (−0.755, +0.205) | 7 | 4.523907×10^{-3} |
| (100.100) | (−0.672, −0.308) | 5 | 3.848197×10^{-3} |
| (101.101) | (−0.623, +0.000) | 3 | 3.895543×10^{-4} |
| (110.110) | (−0.755, −0.205) | 5 | 4.523626×10^{-3} |
| (111.111) | (−0.685, +0.000) | 5 | 2.058372×10^{-3} |

Let us consider the case of $k\ell = 6$ again for the Poincaré map of Duffing equation. From the images of S under T and T^{-3} , we can add the labels to the vertical and horizontal stripes as shown in the top of Fig. 5 according to the manner explained in Sec. 3. Focusing on the basic sequence $b = (100.100)$, we choose the initial condition $\mathbf{x}_0 = (-0.672, -0.308)$. After the fifth iterations of Newton’s method, we could obtain the corresponding UPP within the given error. Also, we obtained further UPPs with the initial conditions as shown in Table 3. These obtained UPPs are shown in Fig. 6. On the trajectories shown in Fig. 6, we can see completely the same topology between each position of UPPs and

the images of S under T . Since the original dynamical system is the continuous-time system defined with $t \in \mathbb{R}$, we can also see the unstable periodic orbits corresponding to the UPPs in \mathbb{R}^2 , as shown in the right-hand side of Fig. 6. There are no problems that some orbits cross each other because the original Duffing equation is a nonautonomous system.

Table 4 shows the eigenvalues for each UPP categorized by the basic sequences. This table includes the cases of $\ell = 2, 4$, and one result for $\ell = 8$ with the basic sequence of 00000001. From the table, our method is also suitable for the UPOs with a much larger value of eigenvalue.

4.2. Controlling chaos by EFC with targeting UPO

Let us do numerical experiments of the Duffing equation (17) to validate the EFC using the UPO obtained by our method. According to Eq. (10), the modified dynamical system after taking account of the controlling part of Fig. 2 is

$$\begin{aligned} \frac{dx}{dt} &= y + K_x(x - x^*(t)), \\ \frac{dy}{dt} &= -\kappa y - x^3 + \gamma_0 + \gamma \cos t + K_y(y - y^*(t)), \end{aligned} \tag{19}$$

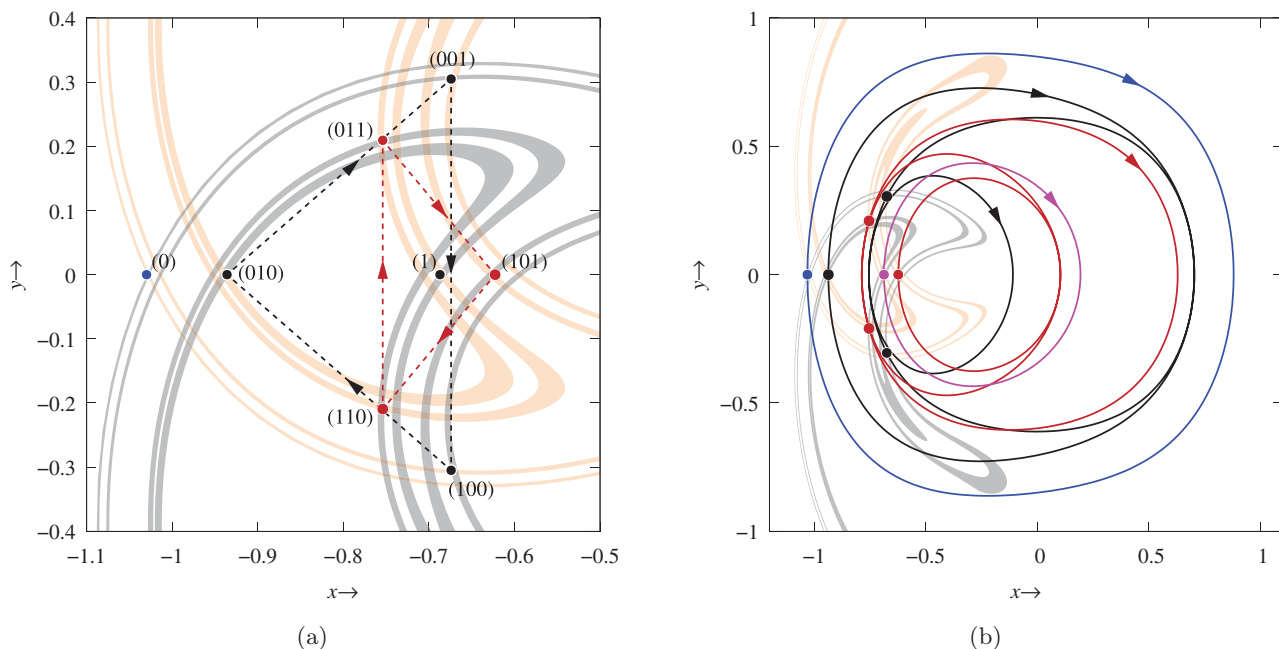


Fig. 6. (a) Numerically calculated periodic points of the Poincaré map of Duffing equation and (b) their corresponding solution orbits.

Table 4. Eigenvalues μ_1 and μ_2 of $DT(\mathbf{p})$ for the Poincaré map of Duffing equation (17). The values having magnitude more than unity are emphasized.

| Basic Sequence | μ_1 | μ_2 |
|----------------|---|---|
| (0) | $+1.982185 \times 10^{-1}$ | $+5.044932$ |
| (1) | -3.356635 | -2.979172×10^{-1} |
| (01) | -9.659009 | -1.035301×10^{-1} |
| (001) | -5.490790×10 | -1.821228×10^{-2} |
| (011) | $+1.982978 \times 10^{-2}$ | $+5.042912 \times 10$ |
| (0001) | -2.787754×10^2 | -3.587107×10^{-3} |
| (0011) | $+3.599590 \times 10^{-3}$ | $+2.778088 \times 10^2$ |
| (0111) | -1.208045×10^2 | -8.277821×10^{-3} |
| (0000001) | $+5.42777707 \times 10^{-6}$ | $+1.84236855 \times 10^5$ |

where K_x and K_y are the gain, and $x^*(t)$ and $y^*(t)$ are the x and y coordinates of target UPO $\mathbf{x}^*(t)$, respectively. In this study, we set the parameters $K_x = K_y = -1$ and the others are the same as the previous section. As the target UPO, let us choose four UPOs such that $\varphi(t, \mathbf{p}_{(0)})$, $\varphi(t, \mathbf{p}_{(01)})$, $\varphi(t, \mathbf{p}_{(001)})$, and $\varphi(t, \mathbf{p}_{(0000001)})$, where \mathbf{p} is the

UPP and its right subscript corresponds to the basic sequence of the obtained UPP. Concretely,

$$\mathbf{p}_{(0)} = (-1.02995193, 0.00000024),$$

$$\mathbf{p}_{(01)} = (-0.70389635, -0.20138366),$$

$$\mathbf{p}_{(001)} = (-0.67405357, 0.30474589),$$

$$\mathbf{p}_{(0000001)} = (-1.027205124082, 0.000000000088).$$

In the experiments, we will switch the system (17) and (19) manually to clarify the effectiveness of the controlling. In other words, we will turn on and off the controlling manually.

Figure 7 shows the result of applying EFC, exhibiting the trajectories of the system state x and the control input $u_x(t) = K_x(x - x^*(t))$. We turn on the controlling from the time $t = 4\ell\pi$ to $t = 20\ell\pi$, where ℓ is the period of the target UPP. All of the cases show that the control input converges to zero quickly. Afterwards, we no longer see the chaotic state and observe the steady state with pretty small amplitude of $u_x(t)$. Even with inputting a tiny control signal, we can see quite different behavior from

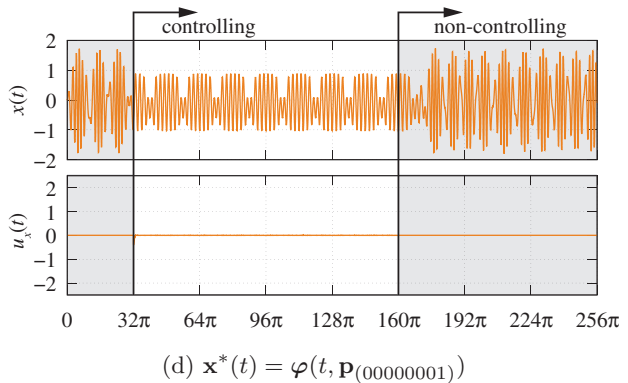
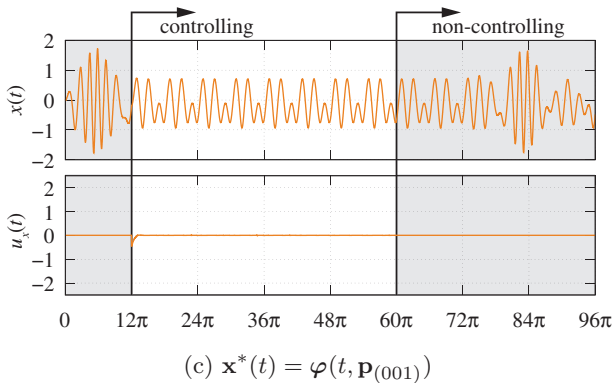
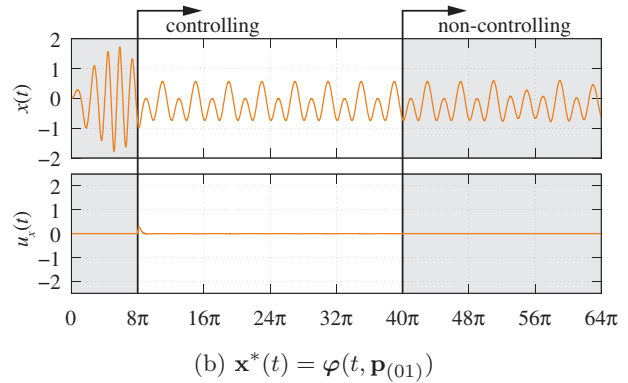
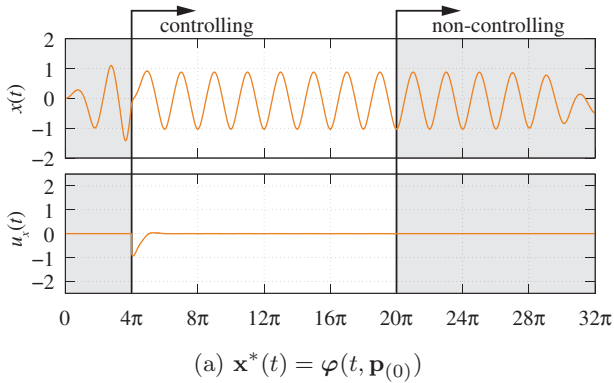


Fig. 7. EFC with targeting UPO. In the top figure of each window, orange trajectory is the trajectory of the modified system (19) and gray one is the trajectory of the original system (19). The gray shaded area in each figure indicates the time interval without controlling.

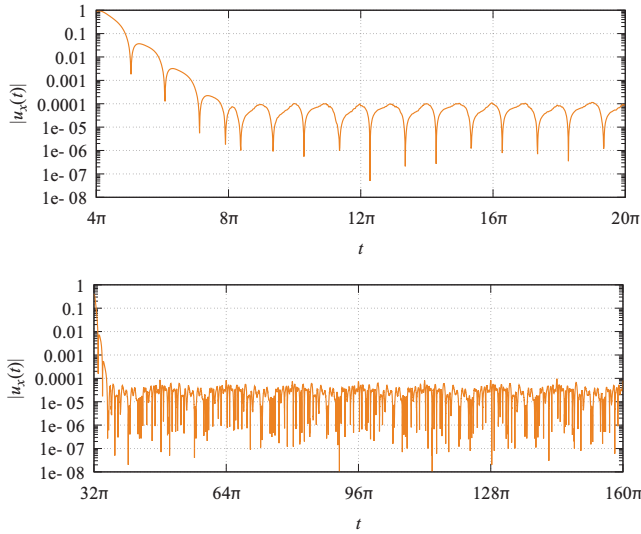


Fig. 8. Transition of the control input in the absolute value with a log scale. Target orbit is (top) $\mathbf{x}^*(t) = \varphi(t, \mathbf{p}_0)$ and (bottom) $\mathbf{x}^*(t) = \varphi(t, \mathbf{p}_{00000001})$.

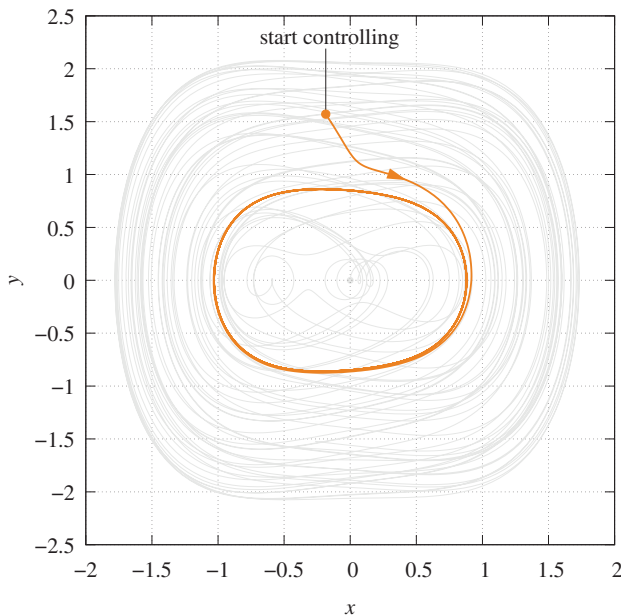
the original system (17). When $t > 20\ell\pi$, after turning off the control input, we cannot observe the steady state found in the controlled situation, and the system again generates chaotic state. Focusing on the cases of Figs. 7(a) and 7(d), Fig. 8 exhibits the transition of the control input in the absolute value, plotted on a log scale. We find that the

control input remains in the range $|u_x(t)| < 10^{-4}$ while the trajectory is in steady state. For the cases with the other target orbits in Fig. 7, we have also confirmed the convergence is to the same extent. As a remarkable feature of Fig. 8(d), the proposing method is still robust when $t = 160\pi$ s has passed even though the target UPP has the instability of $\mu = 1.84236855 \times 10^5$. Besides, Fig. 9 shows the behavior of the controlled trajectory in the state space. From these figures, we can confirm the quick convergence of the trajectory to the steady state. Similarly, we can see that $u_y(t)$ also shrinks quickly.

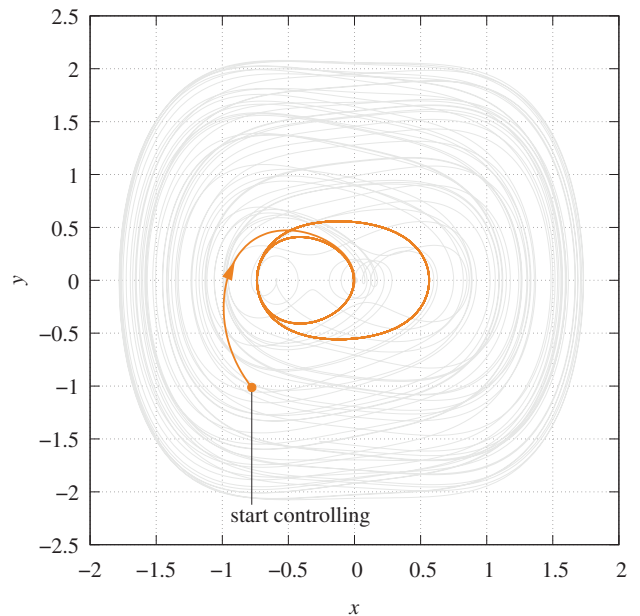
Let us also confirm the robustness of our method for the external input. In the case of $\mathbf{x}^*(t) = \varphi(t, \mathbf{p}_1)$, we do a brief numerical experiment using an external impulse input:

$$\delta(t) = \begin{cases} 2 \cos\left(\frac{t}{16}\right) \cdot \frac{t}{16\pi} & \text{if } t \equiv 0 \pmod{16\pi} \\ 0 & \text{otherwise} \end{cases}$$

to $\mathbf{x}(t)$. Figure 10 shows the result of the experiment. Whatever is the amplitude of the external input applied, we find that the proposing method instantly reacts to the error, and the state converges to the target with precision to the extent of 10^{-4} .



(a) $\mathbf{x}^*(t) = \varphi(t, \mathbf{p}_{(0)})$



(b) $\mathbf{x}^*(t) = \varphi(t, \mathbf{p}_{(01)})$

Fig. 9. EFC with targeting UPOs in the state space. The trajectory in gray is the chaotic state of Eq. (17) with $\mathbf{x}_0 = (0, 0)$ and $t \in (0, 100\pi)$.

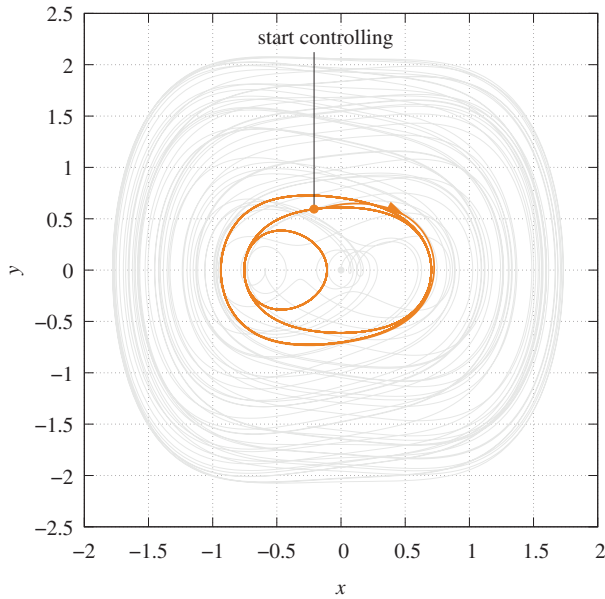
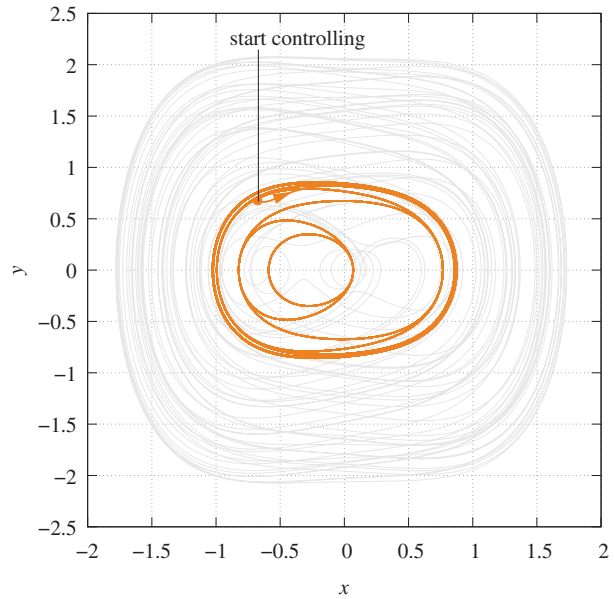
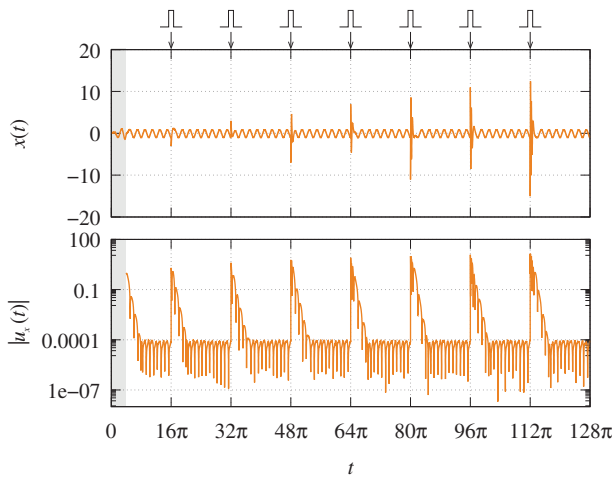

 (c) $\mathbf{x}^*(t) = \varphi(t, \mathbf{p}_{(001)})$

 (d) $\mathbf{x}^*(t) = \varphi(t, \mathbf{p}_{(00000001)})$

Fig. 9. (Continued)


 Fig. 10. EFC with targeting UPOs (impulse interrupted). $\mathbf{x}^*(t) = \varphi(t, \mathbf{p}_1)$.

5. Conclusion

Based on the theory of symbolic dynamical systems, we have proposed a novel computation method to locate and stabilize arbitrary unstable periodic points (UPPs) in the two-dimensional dynamical system with a Smale horseshoe. By introducing the subset based correspondence between the dynamical systems on \mathbb{R}^2 and on a space of symbolic sequences, we have found the region of \mathbb{R}^2 certainly containing a UPP. As the result of a numerical experiment for the Duffing equation, we located the exact coordinates of UPPs. Besides, we have

conducted the numerical experiments of the EFC method targeting the UPO. We confirmed that the proposing EFC shows quick convergence of the chaotic state to the steady state through some numerical experiments. Moreover, we found the control input of the method keeps the value within an extremely small range, 10^{-4} .

For future works, we should try to apply the method to the cases where chaos is attractive. In such a case, we have to consider how can we determine the region S .

Acknowledgment

This study is supported by Takaya Nakanishi and Shohei Miyazaki, who were the research students of Ueta laboratory.

References

- Aihara, K., Takabe, T. & Toyoda, M. [1990] "Chaotic neural networks," *Phys. Lett. A* **144**, 333–340.
- Farantos, S. C. [1995] "Methods for locating periodic orbits in highly unstable systems," *J. Molecul. Struct.: THEOCHEM* **341**, 91–100.
- Habutsu, T., Nishio, Y., Sasase, I. & Mori, S. [1990] "A secret key cryptosystem using a chaotic map," *IEICE Trans.* **E73**, 1041–1044.
- Huang, T., Han, X. & Lu, J. [2008] "Chaos predication method based on Lyapunov exponent and its application in water quality forecast," *J. Xi'an Univ. Architect. Technol. (Nat. Sci. Ed.)* **40**, 846–851.

- Kittel, A., Parisi, J. & Pyragas, K. [1995] “Delayed feedback control of chaos by self-adapted delay time,” *Phys. Lett. A* **198**, 433–436.
- Kovacic, I. & Brennan, M. J. [2011] *The Duffing Equation: Nonlinear Oscillators and Their Behaviour* (John Wiley & Sons).
- Mahmoud, G. M., Arafa, A. A., Abed-Elhameed, T. M. & Mahmoud, E. E. [2017] “Chaos control of integer and fractional orders of chaotic Burke–Shaw system using time delayed feedback control,” *Chaos Solit. Fract.* **104**, 680–692.
- Myneni, K., Barr, T., Corron, N. & Pethel, S. [1999] “New method for the control of fast chaotic oscillations,” *Phys. Rev. Lett.* **83**, 2175.
- Nakajima, H. [1997] “On analytical properties of delayed feedback control of chaos,” *Phys. Lett. A* **232**, 207–210.
- Ott, E., Grebogi, C. & Yorke, J. [1990] “Controlling chaos,” *Phys. Rev. Lett.* **64**, 1196.
- Pyragas, K. [1992] “Continuous control of chaos by self-controlling feedback,” *Phys. Lett. A* **170**, 421–428.
- Rajasekar, S. & Lakshmanan, M. [1993] “Algorithms for controlling chaotic motion: Application for the BVP oscillator,” *Physica D* **67**, 282–300.
- Sabuco, J., Zambrano, S. & Sanjuán, M. [2010] “Partial control of chaotic transients using escape times,” *New J. Phys.* **12**, 113038.
- Smale, S. [2000] “Diffeomorphisms with many periodic points,” *The Collected Papers of Stephen Smale: Volume 2* (World Scientific), pp. 636–653.
- Stojanovski, T. & Kocarev, L. [2001] “Chaos-based random number generators-part I: analysis [cryptology],” *IEEE Trans. Circuits Syst.* **48**, 281–288.
- Ueta, T., Ito, D. & Aihara, K. [2015] “Can a pseudo periodic orbit avoid a catastrophic transition?” *Int. J. Bifurcation and Chaos* **25**, 1550185-1–10.
- Yi, L., Liu, Y. & Yu, W. [2019] “Combination of improved OGY and guiding orbit method for chaos control,” *J. Adv. Comput. Intell. Intell. Inform.* **23**, 847–855.
- Zambrano, S. & Sanjuán, M. [2009] “Exploring partial control of chaotic systems,” *Phys. Rev. E* **79**, 026217.